DIGITAL ACCESS TO SCHOLARSHIP AT HARVARD
DASH.HARVARD.EDU

HARVARD LIBRARY
Office for Scholarly Communication

In vivo Brillouin optical microscopy of the human eye

Citation
Scarcelli, Giuliano, and Seok Hyun Yun. 2012. In vivo brillouin optical microscopy of the human eye. Optics Express 20(8): 9197-9202.

Published Version
doi:10.1364/OE.20.009197

Permanent link
http://nrs.harvard.edu/urn-3:HUL.InstRepos:11179746

Terms of Use
This article was downloaded from Harvard University's DASH repository, and is made available under the terms and conditions applicable to Other Posted Material, as set forth at http://nrs.harvard.edu/urn-3:HUL.InstRepos:dash.current.terms-of-use#LAA

Share Your Story

The Harvard community has made this article openly available.
Please share how this access benefits you. Submit a story .

Accessibility

In vivo Brillouin optical microscopy of the human eye

Giuliano Scarcelli and Seok Hyun Yun*

Harvard Medical School and Wellman Center for Photomedicine, Massachusetts General Hospital, 50 Blossom St., BHX-6, Boston, Massachusetts 02114, USA

**syun@hms.harvard.edu*

Abstract: We report the first Brillouin measurement of the human eye *in vivo*. We constructed a Brillouin optical scanner safe for human use by employing continuous-wave laser light at 780 nm at a low power of 0.7 mW. With a single scan along the optic axis of the eye, the axial profile of Brillouin frequency shift was obtained with a pixel acquisition time of 0.4 s and axial resolution of about 60 μm, showing the depth-dependent biomechanical properties in the cornea and lens.

©2012 Optical Society of America

OCIS codes: (300.6190) Spectrometers; (290.5830) Scattering, Brillouin.

References and links

1. G. Scarcelli and S. H. Yun, "Confocal Brillouin microscopy for three-dimensional mechanical imaging," Nat. Photonics **2**(1), 39–43 (2008).
2. X. Bao, M. DeMerchant, A. Brown, and T. Bremner, "Tensile and compressive strain measurement in the lab and field with the distributed Brillouin scattering sensor," J. Lightwave Technol. **19**(11), 1698–1704 (2001).
3. G. D. Hickman, J. M. Harding, M. Carnes, A. Pressman, G. W. Kattawar, and E. S. Fry, "Aircraft laser sensing of sound velocity in water: Brillouin scattering," Remote Sens. Environ. **36**(3), 165–178 (1991).
4. J. Randall and J. M. Vaughan, "The measurement and interpretation of Brillouin scattering in the lens of the eye," Proc. R. Soc. Lond. B Biol. Sci. **214**(1197), 449–470 (1982).
5. J. M. Vaughan and J. T. Randall, "Brillouin scattering, density and elastic properties of the lens and cornea of the eye," Nature **284**(5755), 489–491 (1980).
6. G. Scarcelli and S. H. Yun, "Multistage VIPA etalons for high-extinction parallel Brillouin spectroscopy," Opt. Express **19**(11), 10913–10922 (2011).
7. S. Reiß, G. Burau, O. Stachs, R. Guthoff, and H. Stolz, "Spatially resolved Brillouin spectroscopy to determine the rheological properties of the eye lens," Biomed. Opt. Express **2**(8), 2144–2159 (2011).
8. G. Scarcelli, P. Kim, and S. H. Yun, "In vivo measurement of age-related stiffening in the crystalline lens by Brillouin optical microscopy," Biophys. J. **101**(6), 1539–1545 (2011).
9. S. T. Bailey, M. D. Twa, J. C. Gump, M. Venkiteshwar, M. A. Bullimore, and R. Sooryakumar, "Light-scattering study of the normal human eye lens: elastic properties and age dependence," IEEE Trans. Biomed. Eng. **57**(12), 2910–2917 (2010).
10. G. Scarcelli, R. Pineda, and S. H. Yun, "Brillouin optical microscopy for corneal biomechanics," Invest. Ophthalmol. Vis. Sci. **53**(1), 185–190 (2012).
11. C. R. Ethier, M. Johnson, and J. Ruberti, "Ocular biomechanics and biotransport," Annu. Rev. Biomed. Eng. **6**(1), 249–273 (2004).
12. G. Scarcelli, P. Kim, and S. H. Yun, "Cross-axis cascading of spectral dispersion," Opt. Lett. **33**(24), 2979–2981 (2008).
13. D. Sliney, D. Aron-Rosa, F. DeLori, F. Fankhauser, R. Landry, M. Mainster, J. Marshall, B. Rassow, B. Stuck, S. Trokel, T. M. West, and M. Wolffe; International Commission on Non-Ionizing Radiation Protection, "Adjustment of guidelines for exposure of the eye to optical radiation from ocular instruments: statement from a task group of the international commission on non-ionizing radiation Protection (ICNIRP)," Appl. Opt. **44**(11), 2162–2176 (2005).
14. T. Okuno, M. Kojima, I. Hata, and D. H. Sliney, "Temperature rises in the crystalline lens from focal irradiation," Health Phys. **88**(3), 214–222 (2005).
15. F. C. Delori, R. H. Webb, and D. H. Sliney; American National Standards Institute, "Maximum permissible exposures for ocular safety (ANSI 2000), with emphasis on ophthalmic devices," J. Opt. Soc. Am. A **24**(5), 1250–1265 (2007).
16. C. E. Jones, D. A. Atchison, R. Meder, and J. M. Pope, "Refractive index distribution and optical properties of the isolated human lens measured using magnetic resonance imaging (MRI)," Vision Res. **45**(18), 2352–2366 (2005).

#163291 - $15.00 USD Received 21 Feb 2012; revised 30 Mar 2012; accepted 1 Apr 2012; published 5 Apr 2012

17. are A. de Castro, D. Siedlecki, D. Borja, S. Uhlhorn, J.-M. Parel, F. Manns, and S. Marcos, "Age-dependent variation of the gradient index profile in human crystalline lenses," J. Mod. Opt. **58**(19-20), 1781–1787 (2011).
18. M. Kohlhaas, E. Spoerl, T. Schilde, G. Unger, C. Wittig, and L. E. Pillunat, "Biomechanical evidence of the distribution of cross-links in corneas treated with riboflavin and ultraviolet A light," J. Cataract Refract. Surg. **32**(2), 279–283 (2006).
19. J. B. Randleman, D. G. Dawson, H. E. Grossniklaus, B. E. McCarey, and H. F. Edelhauser, "Depth-dependent cohesive tensile strength in human donor corneas: implications for refractive surgery," J. Refract. Surg. **24**(1), S85–S89 (2008).
20. C. L. De Korte, A. F. W. Van Der Steen, J. M. Thijssen, J. J. Duindam, C. Otto, and G. J. Puppels, "Relation between local acoustic parameters and protein distribution in human and porcine eye lenses," Exp. Eye Res. **59**(5), 617–627 (1994).
21. S. J. McGinty and R. J. W. Truscott, "Presbyopia: the first stage of nuclear cataract?" Ophthalmic Res. **38**(3), 137–148 (2006).
22. C. Roberts, "The cornea is not a piece of plastic," J. Refract. Surg. **16**(4), 407–413 (2000).
23. D. A. Luce, "Determining in vivo biomechanical properties of the cornea with an ocular response analyzer," J. Cataract Refract. Surg. **31**(1), 156–162 (2005).
24. B. M. Fontes, R. Ambrósio, Jr., G. C. Velarde, and W. Nosé, "Ocular response analyzer measurements in keratoconus with normal central corneal thickness compared with matched normal control eyes," J. Refract. Surg. **27**(3), 209–215 (2011).
25. A. Glasser and M. C. W. Campbell, "Biometric, optical and physical changes in the isolated human crystalline lens with age in relation to presbyopia," Vision Res. **39**(11), 1991–2015 (1999).

1. Introduction

Brillouin optical microscopy is a novel technique based on Brillouin light scattering spectroscopy for probing the viscoelastic properties of a sample with three-dimensional resolution [1]. Brillouin spectroscopy has long been applied for material characterization and environmental sensing [2, 3]. The first Brillouin spectroscopy of biological tissues was demonstrated in the early 1980s [4, 5], where the Brillouin spectra of lens and cornea at single spatial points were obtained with an integration time of 10 min to 1 hour. The recent development of parallel spectrometer drastically reduced the acquisition time to 1 s or less [6], which allowed spatially resolved measurements [1, 7] and imaging [8]. An *in vivo* study of murine lenses revealed age-related changes in the Brillouin profiles of the lens nucleus and also found an empirical relationship between the Brillouin modulus and conventional Young's modulus [8]. Spatially-resolved measurements of human lenses [9] and animal corneas *ex vivo* [10] were recently demonstrated.

The possibility of applying the technique to a living patient offers an exciting opportunity for early detection of ocular problems, such as presbyopia and corneal ectasia, and for understanding their underlying mechanisms [11]. Here, we report the development of a clinically viable Brillouin microscope and describe the first Brillouin measurement of the human eye *in vivo*. For human use, the instrument employs a low-power laser light at 780 nm and a parallel Brillouin spectrometer optimized for the infrared wavelength.

2. Setup and methods

Figure 1 shows a schematic of the experimental setup. The instrument is comprised of three parts: laser-scanning confocal microscope, human interface, and VIPA-etalon spectrometer. The light source was a continuous-wave (cw) external-cavity semiconductor laser emitting a single longitudinal mode at 780 nm (Toptica Photonics). The laser output was attenuated with a neutral density filter and expanded to the $1/e^2$ laser beam diameter of about 7 mm. A 10/90 beam sampler directed 10% of the laser power to the human interface through a beam-scanning unit. We used two mirrors for x-y transverse beam positioning and a motorized translation stage (max speed 1.5 cm/s, Zaber Technologies) for z-scan. We used two different objective lenses: an achromat (Thorlabs, f = 35 mm, NA = 0.055) with a long working distance (35 mm) was used; and a 4X microscope objective (Edmund Optics, NA = 0.1) with higher spatial resolution was utilized. The backward scattered light from the eye was collected with a single-mode optical fiber through the beam sampler (90% transmission). We used two-stage VIPA etalons optimized for the near-infrared wavelength (R1 = 99.9%, R2 = 98% at

#163291 - $15.00 USD Received 21 Feb 2012; revised 30 Mar 2012; accepted 1 Apr 2012; published 5 Apr 2012
(C) 2012 OSA

760-800 nm), configured with the cross-axis cascade principle [12]. In each stage, the light beam was line-focused into the input window of the VIPA etalon tilted by about 2 degrees and the output pattern went through a spatial filter to remove the elastic scattering light component. The spectrally dispersed pattern was imaged onto an EM-CCD camera (Andor, IXon DU-897). The camera was operated at full gain with a negligible readout noise.

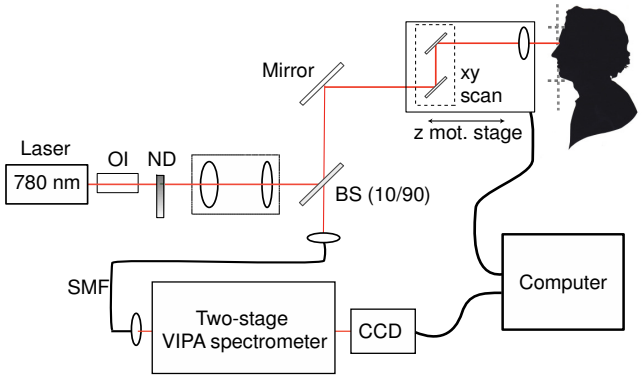

Fig. 1. Schematic of the Brillouin confocal microscope. OI: Optical isolator. ND: Neutral density filter wheel; BS: beam sampler; SMF: single mode fiber.

The human interface was a modified version of standard ophthalmic slit-lamp instrument. It has a chin support and a headrest, which allowed the height of the head of the human subject to be adjusted with a manual translation stage. All measurements were performed in the relaxed accommodation state. Prior to the Brillouin scan, we aligned the position of the beam to the corneal apex by finding the location that maximizes the optical back-reflection from the corneal surface. The focus of the laser beam was scanned along the optical axis from the cornea to the lens or backward. Axial scanning was performed by moving the objective lens with speeds ranging between 30 and 80 μm/s. The Brillouin spectra were recorded in the CCD camera with the frame integration times between 0.2 and 1 s. The laser power at the sample could be adjusted between 0.7 and 3mW. Beam scanning, CCD acquisition and spectral analysis were synchronized with LABVIEW and MATLAB programs. The measurement results were displayed in real-time on a computer. The axial profile of the Brillouin shift was plotted with respect to the focal depth in the eye, calculated using the average refractive index (n = 1.4) of the eye anterior chamber, which was measured by a low-coherence interferometer.

3. Safety consideration

We considered radiation-induced damage thresholds in the retina, as well the cornea and lens. Maximum permissible exposure (MPE) is defined as the highest power or energy density that can be admitted to the eye without causing a biohazard. MPE corresponds to 10% of the dose that has a 50% chance of creating damage in worst-case scenario conditions. In the Brillouin scanner, the laser light is focused in the anterior segment and diffused onto the retina (Fig. 2). According to the International Commission on Non-Ionizing Radiation Protection (ICNIRP), for cw sources in the wavelength region 400-1050 nm the exposure limit for cornea-lens thermal safety is 4W/cm^2; i.e. MPE = 32 mW in a 1-mm-diameter zone (0.79 mm^2 in area) [13]. The 1-mm aperture for irradiance averaging is based on the thermal modeling [14], which shows that the temperature rise is independent of the beam size up to 1 mm due to rapid thermal conduction (~0.5 W/m/°C) in the cornea and lens. As for the retina, the dominant mechanism of retinal damage is thermal for an exposure time (T) longer than 0.25 s. Considering the distance 17 mm between the lens and retina and α = 0.2, i.e. NA = 0.1, the beam size on the retina is >3 mm. Applying the same thermal limit of 4 W/cm^2,we calculate

#163291 - $15.00 USD Received 21 Feb 2012; revised 30 Mar 2012; accepted 1 Apr 2012; published 5 Apr 2012
(C) 2012 OSA

MPE = ~300 mW. According to the guidelines from American National Standard Institute, the exposure limit for the retinal thermal hazard has been expressed as $1.8\text{x}10^{-3} C_A\ C_E\ T^{-0.25}$ [W/cm^2], where C_A = 1.45 (for = 780 nm), C_E = 267 (for α = 0.2; i.e. NA = 0.1), and the aperture size of 7mm (area of 0.38 cm^2) [15].The MPE is calculated to be 265 mW for T = 1 sand 95 mW for T = 60 s, which is consistent with the above analysis. Taken together, we conclude that the Brillouin scan in the cornea and lens does not pose risk to the human eye.

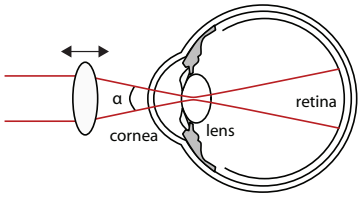

Fig. 2. Laser illumination in the Brillouin scanner. By focusing the beam in the transparent tissue of the anterior chamber (cornea, aqueous humor and lens), the beam is diverging and covers a large area when it hits the retina.

4. Results

The experimental protocol has been reviewed and approved by the Institutional Review Board for human research at the Massachusetts General Hospital. A 42-year-old male healthy volunteer was enrolled. Prior to the Brillouin test, a full eye exam including topography and pachymetry was conducted, which did not reveal any abnormality and measured a central corneal thickness of 530 μm. The optical power used in the Brillouin scan was measured to be 0.7 mW at the eye, about 50 times lower than the MPE.

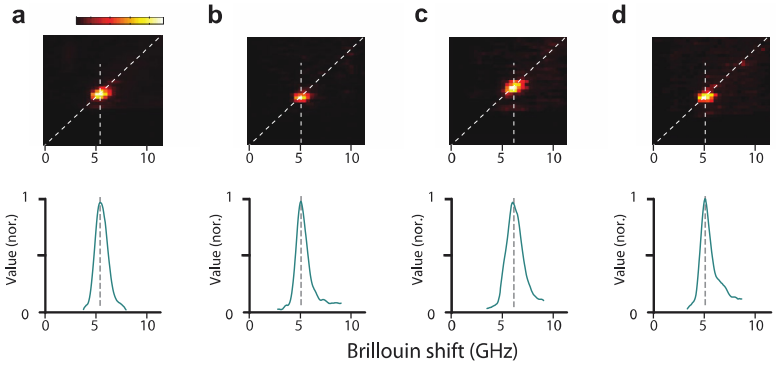

Fig. 3. Representative Brillouin spectra (anti-Stokes peaks) from a human eye. (a) Corneal stroma. (b) Aqueous humor. (c) Lens nucleus. (d) Vitreous humor. Top panels: raw CCD spectra (average of four frames). Bottom panels: corresponding spectra.

Figure 3 shows representative spectra acquired in four regions of the eye: cornea, aqueous humor, lens nucleus and vitreous humor, respectively. The top panels are raw CCD images featuring anti-Stokes Brillouin scattering light, and the bottom panels are the corresponding Brillouin spectra extracted from the CCD frames by the image analysis that has been described elsewhere [6,8]. Briefly, a reference arm (not shown in Fig. 1) periodically interrogates samples, such as water and PMMA, of known Brillouin frequency shifts. From the reference spectra, the direction of the spectral dispersion axis (diagonal lines) and its pixel-to-GHz ratio are measured (0.38 GHz/pixel). To obtain the spectrum along the spectral dispersion axis, the CCD images are interpolated (x4) and integrated over the orthogonal axis. The Brillouin frequency shift is determined with Lorentzian curve fitting. The measurement sensitivity of the Brillouin peak detection was measured to be 30-120 MHz for this data set.

#163291 - $15.00 USD Received 21 Feb 2012; revised 30 Mar 2012; accepted 1 Apr 2012; published 5 Apr 2012
(C) 2012 OSA

Figure 4 shows the measured axial profile obtained from the left eye of the volunteer. For Brillouin scan, the beam focus was translated along the optic axis of the eye at a speed of 50 μm/s (in air), and the Brillouin spectra were acquired with a CCD frame rate of 2.5 Hz (i.e. integration time of 0.4 s). The axial profile of the lens shown in Fig. 4(a) was obtained with the 35-mm achromatic lens with an axial resolution of about 350 μm. It features a typical bell shape with a slope in the anterior cortex, a plateau at about 6.05 GHz in the lens nucleus, and a decline in the posterior cortex towards the vitreous humor. The axial profile shown in Fig. 4(b) was obtained with the 4X objective at a higher axial resolution of ~60 μm. It reveals a better resolved anterior cortex of the lens, with the Brillouin shift varying steeply from 5.25 GHz to 5.85 GHz in the initial 300 μm layer. The high-resolution scan also allowed us to obtain the Brillouin profile of the cornea. Between 100 μm and 400 μm depths, corresponding to the corneal stroma, the Brillouin shift declined slowly from ~5.6 GHz to ~5.5 GHz. In the posterior region of the cornea, the Brillouin profile showed a steeper decline from 5.5 GHz to 5.25 GHz in about 200 μm. With the finite confocal resolution, strong Fresnel reflection from the corneal surface made it difficult to analyze the first 70 μm from the corneal surface. The aqueous humor was measured to have a fairly constant Brillouin frequency, slightly higher than the Brillouin shift of pure water.

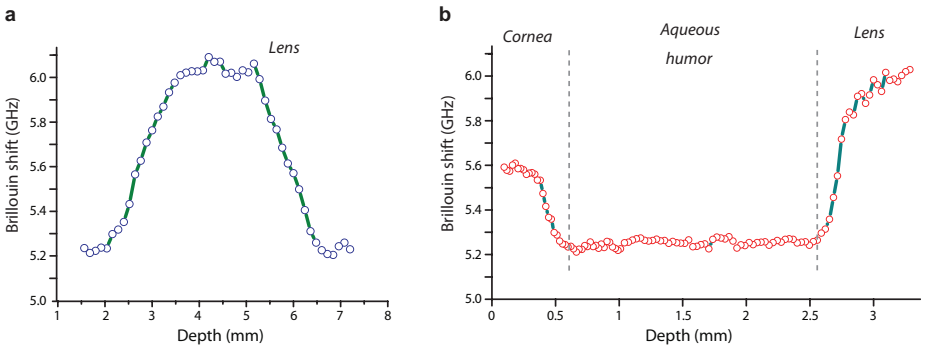

Fig. 4. *In vivo* Brillouin measurement of a human eye. (a) Depth profile of the crystalline lens. (b) Depth profile of the anterior chamber. The data are an average of four such scans taken ten minutes apart.

We performed a total of four scans on the same subject within the span of one month. The variation of the Brillouin shift in the aqueous humor was measured to be about 30 MHz. As per approved protocol, at eight months after the Brillouin tests the subject underwent a follow-up full eye exam. As expected, the results showed no abnormalities and no changes in static or dynamic visual acuity.

6. Discussion

The measured Brillouin frequency shifts of the human lens and cornea *in vivo* agreed well with previous measurements of *ex vivo* tissues. Vaughan and Randall reported Brillouin shifts of 4.54 GHz, 4.71 GHz, and 4.71 GHz for cornea, cortex and nucleus, respectively [4, 5]. Bailey et al. reported Brillouin shifts of 7.75 GHz (cortex) and 8.8 GHz (nucleus) [9]. Brillouin shift, Ω, can be written as $\Omega = 2n/\lambda\sqrt{M/\rho}\cos(\theta/2)$ where n, M, and ρ are the refractive index, longitudinal elastic modulus (hereinafter "Brillouin" modulus), and density, respectively, λ is the wavelength of probe light, and θ is the angle between incident and scattered light. For comparison, we converted the Brillouin shifts to Brillouin modulus M using n = 1.37, 1.37 and 1.42, and ρ = 1.11, 1.06 and 1.11 g/ml for cornea, cortex and nucleus, respectively [4, 16]. For cornea, the modulus is computed to be 2.7 GPa [4]; for cortex, the moduli are 2.8 GPa [4, 5], and 2.36 ± 0.09 GPa [9]; for nucleus, 2.93 GPa [4, 5], and 2.79 ± 0.14 GPa [9]. In our measurements corneal Brillouin modulus ranged from 2.82 to 2.5 GPa

#163291 - $15.00 USD Received 21 Feb 2012; revised 30 Mar 2012; accepted 1 Apr 2012; published 5 Apr 2012
(C) 2012 OSA

and the lens Brillouin moduli varied between 2.38 and 3.1 GPa. These values are consistent with the values reported by Vaughan and Bailey et al [5, 9]. One caveat in this analysis is that literature data on index and density are variable, in part because index and density vary within the ocular tissues [16, 17]. Thus, the conversion to Brillouin modulus has an uncertainty by 2-3%.

Our data showed a marked depth dependence of longitudinal modulus in the cornea and lens. Previous mechanical tests hinted at elasticity gradient within both cornea and lens tissue. Kohlhaas et al. measured the anterior corneal stroma to have three times higher Young's modulus than the posterior stroma [18]. Randleman et al. reported that the elastic modulus decreased from the front to the back of the cornea [19], consistent with our *in vivo* data and previous animal data [10]. As for the lens, the crystalline proteins are packed with increasingly tighter density toward the nucleus so that a varying modulus is expected. The increase in density of crystalline proteins was measured in animals [20]. The spatial variation of Brillouin modulus has been reported in the lens in animals *ex vivo* [7] and *in vivo* [8].

Brillouin modulus differs from quasi-static Young's modulus from a fundamental point of view. For a biological tissue with high water content, the Brillouin modulus is much higher than Young's modulus. This effect produced an apparently counterintuitive result: while the corneal tissue is known to have higher Young's modulus than the lens tissue, the Brillouin modulus of the cornea is actually lower mostly because of the higher water content in the cornea (~80%) than in the lens (~65%). Nevertheless, a good correlation can be found between Brillouin modulus and Young's modulus for the same tissue type [8].

The biomechanical properties of the lens and cornea have been linked to various ocular disorders. Presbyopia is thought to occur due to the age-related stiffening of the lens. Although Brillouin microscopy was shown to be able to detect age-related stiffening in animals [8], its ability to detect this effect in human lenses has been questioned [9]. Stiffening of the human lens has also been linked to the onset of age-related nuclear cataracts [21]. As for the cornea, keratoconus and corneal ectasia are associated to a reduced corneal modulus [22]. However, current clinical analysis of the eye is limited to structural measurements while traditional mechanical tests are destructive and cannot be employed in clinical settings. The only instrument for corneal mechanical analysis is the ocular response analyzer (ORA) [23], but its sensitivity and clinical usefulness are still under question [24].

The spatial resolution of the current Brillouin scanner does not allow us to single out the Brillouin scattering signature of the lens capsule. The contribution of the capsule to the accommodative amplitude has been studied, although the mechanical modulus of the capsule may not change much with age [25]. Using a higher-NA objective lens, it may be possible to resolve the capsule and measure its Brillouin modulus. Another limitation of current Brillouin instrument for use in the clinic is the relatively long acquisition time. A single full axial scan across the eye takes about 1 min, although the scan time could be reduced to <10 s at the expense of the scan range or sampling intervals. By reducing the optical loss in the spectrometer and improving VIPA etalon coating procedures, it might be possible to decrease the spectral acquisition time by 10 fold and thereby to obtain several axial or transverse scans across the lens. This speed improvement will help to assess the equatorial distribution of the elastic modulus of the lens.

Acknowledgments

The authors thank Dr. Puoris'haag for help in writing the study protocol and Dr. Roberto Pineda at Massachusetts Eye and Ear Infirmary for performing the eye exams. This work was supported by the National Institutes of Health (R21EB008472, P41RR032042), National Science of Foundation (CBET-0853773), Department of Defense (FA9550-04-1-0079), and the Center for Integration of Medical Innovation and Technology.